6th European Conference on Computational Mechanics (ECCM 6)
7th European Conference on Computational Fluid Dynamics (ECFD 7)
1115 June 2018, Glasgow, UK

SENSITIVITY ANALYSIS OF SUPERSONIC TURBINE TRAILING EDGES

Alejandro Martinez-Cava[1], Eusebio Valero[2] and Javier de Vicente[3]

School of Aeronautical and Space Engineering, Universidad Politécnica de Madrid.
Plaza Cardenal Cisneros 3, E-28040, Madrid, Spain
Email: [1]alejandro.martinezcava@upm.es, [2]eusebio.valero@upm.es, [3]fj.devicente@upm.es
Web page: https://ssemid-itn.eu

Key words: BiGlobal, Sensitivity, Turbomachinery, Stability analysis

Abstract. The use of compact architectures on aircraft turbine engines challenges the design and management of structural and thermal load requirements. Even operating in subsonic conditions, supersonic regimes may develop at the high pressure turbine passages, experiencing complex compression and expansion wave systems that interact with adjacent stages of the turbine. When cooling flow is ejected through the blade trailing edge slots, non-symmetrical configurations can appear due to the interaction of the injected flow with the surrounding flow field, leading to undesired loads and efficiency loses. In this work, a combination of RANS simulations, global stability and sensitivity analysis is employed to identify and explain the physical mechanisms of this phenomenon. A global mode associated with the geometrical expansion of the trailing edge slot is identified, and linked to the non-symmetrical configurations. To conclude, the regions where the flow would be more sensitive to flow modifications to excite or damp this phenomena are identified throughout an adjoint approximation.

1 INTRODUCTION

With aircraft engines going towards the use of more compact architectures, structural safety limits and aero-structural couplings can become the bottleneck of engine design due to low and high cycle fatigue issues. The aero-structural interaction become significantly detrimental when flow velocities approach the speed of sound. Engine turbine blades can operate in transonic or supersonic flow regime, specially over high pressure turbine passages where the flow expand to supersonic velocities experiencing complex shock wave systems at the trailing edge. These waves can interact with downstream stages of the turbine affecting the aerodynamic efficiency of the blades and reducing the life-span of the engine components [1]. Up to 30% of total loses on transonic turbines are due to these shock interactions [2], having their origin on the flow fluctuations that take place at the area adjacent to the blades trailing edges, normally referred as the base region.

The flow field around the base region can be summarized in Figure 1-left, where the flow features appearing on a supersonic turbine blade are represented. The upstream boundary layer remains attached at the trailing edge corner, and separates downstream developing a shear layer while, simultaneously, the main flow accelerates through a Prandtl-Meyer expansion fan. Furthermore, a weak compression wave, called separation or lip shock, is formed at the point of flow detachment in order to adapt the pressure gradient between the shearing and the downstream flow. The upper and lower shear layers propagate downstream and eventually merge at the wake on a point of confluence, creating a dead air zone limited by both shear layers and the blunt trailing edge, namely the base region. This zone is characterized by low momentum and constant pressure, having a strong influence on several features of the surrounding flow field. At the confluence point, the flow changes its direction notably, being forced to compress through a system of strong trailing edge shocks. The degree of compression, hence the strength and angle of the shock waves, highly depends on the base region properties.

The nature of the surrounding flow field produces a heavy thermal loading over the turbine blades, requiring heavy cooling systems to avoid the melting of the components. The thin trailing edge cannot be protected using internal cooling passages, so cooler flow bled from the high pressure compressor is purged through slots or orifices to avoid the melting of the turbine components. As it has been shown by several authors [3, 4], this cooling could be exploited to modulate the base region properties. Different studies have been devoted to examine the effects of trailing edge bleeding on the base region. Of particular importance, Saracoglu et al. [5] investigated the flow topology at the blunt trailing edge as a function of the cooling flow intensity, showing the dependence of the base pressure with the blowing magnitude. A relevant result of the study was the presence of non-symmetric configurations at the base flow (shock wave intensity and angle) for a specific range of blowing intensities (Figure 1-right). This work aims to explain these non-symmetric configurations, using stability and sensitivity analysis.

Stability analysis studies the growth or decay of perturbations superimposed upon a steady base flow, and has proven to be effective in the analysis of incompressible and compressible flows, either in laminar or turbulent configurations [6, 7]. The analysis aims

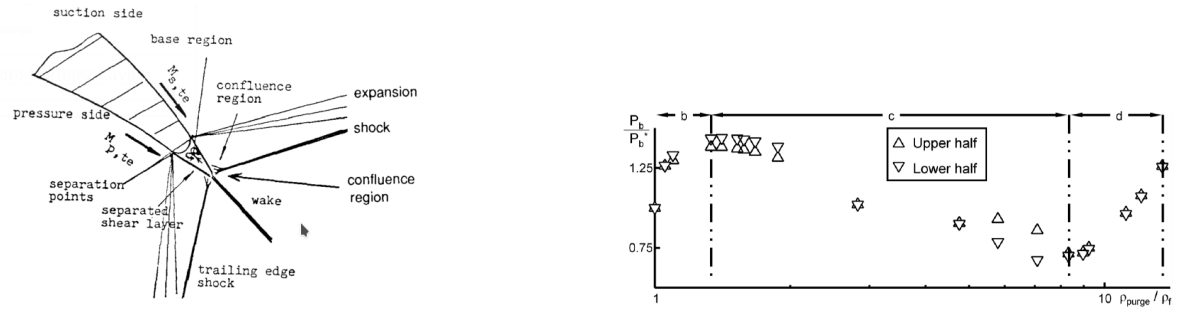

Figure 1: Schematic representation of supersonic flow on a blunt trailing edge (left)[2], and base pressure correlation at the trailing edge as a function of the density ratio of the bleeding rate (right)[5].

to identify which features can naturally appear in the flow and become dominant for some particular value of the parameters. This work combines RANS simulations and linear stability theory to explain the mechanisms that generate the described non-symmetric configuration. A thorough analysis of the flow topology is carried, showing how the recirculation areas aft the trailing edge interact generating changes on the injected flow direction and therefore in the shock wave system. The physical mechanisms responsible of those changes, dependent on the cooling flow purge intensity, are then identified using global stability analysis, matching the bifurcation predicted by the RANS simulations. The unstable configuration seems to be related to the sudden geometrical expansion at the end of the cooling slot. The associated instability forces the purge flow direction to change its direction impacting on one of the trailing edge end shear layers, generating an additional shock wave upstream the main trailing edge shock. The identified global mode changes its structure with the cooling flow intensity, as does the flow topology of the base region, giving valuable information about where the perturbations are located. Furthermore, the additional solution of the adjoint problem and the sensitivity analysis over the case of study allow to identify those areas of the flow field more receptive to structural changes or flow modifications, in order to excite or damp the perturbations responsible of the non-symmetry.

The rest of the paper is organized as follows. Section II overviews the mathematical formulation of the stability and sensitivity analysis, section III summarizes the numerical procedures to obtain the base flow and global modes, in section IV the main results are described, finishing in section V with the main conclusions of this study.

2 MATHEMATICAL MODEL

2.1 Flow solver

The compressible version of the Reynolds Averaged Navier-Stokes equations (RANS) is used to model the flow, closing the mathematical system with the Wilcox $k-\omega$ turbulence model. These set of equations can be written in conservative form as:

$$\frac{\partial}{\partial t}\int_{\Omega}\mathbf{q}d\Omega = -\int_{\partial\Omega}\bar{\bar{F}}\cdot\mathbf{n}dS, \tag{1}$$

where vector[1] $\mathbf{q}$ comprises the conservative variables (density, momentum and energy) and turbulent quantities, while Ω is a control volume with boundary $\partial\Omega$ and outer normal $\mathbf{n}$. $\bar{\bar{F}}$ denotes the flux density tensor, which can be decomposed along the three cartesian coordinate directions and comprises the inviscid, viscous and turbulent fluxes.

The finite volume DLR TAU-Code was used to obtain a steady state solution of the base flow equations. The flow domain Ω is discretized into a finite number of subdomains $\Omega_i, i = 1 \dots N$, where each subdomain contains $\mathcal{N}_f$ faces. The time-accurate three-dimensional Navier-Stokes equations are marched in time towards a steady state using a backward Euler implicit scheme, solved approximately by a LU-SGS (*Lower-Upper Symmetric-Gauss-Seidel Method*) iterations procedure. Local time stepping and multigrid algorithms were adopted to accelerate convergence, allowing to converge a forced-steady solution of the RANS equations from flow configurations that would otherwise develop an unsteady behavior if run with an unsteady solver.

Thus, following the method of lines, the spatial discretization of system (1) gives rise to a system of ordinary differential equations, that can be written in general form for a subdomain Ω_i as:

$$|\Omega|_i \frac{\partial \mathbf{q}_i}{\partial t} + \mathbf{R}_i = \mathbf{0} \quad , \qquad \mathbf{R}_i = \sum_{j=1}^{\mathcal{N}_f} \bar{\bar{F}}_j \mathbf{n}_j, \qquad i = 1 \dots N \tag{2}$$

where $\mathbf{R}_i$ is the residual in subdomain Ω_i, equivalent to the flux contributions to this subdomain, and $\mathbf{q}_i$ represents a discretized vector state solution in subdomain Ω_i. Vectors $\mathbf{q}_i$ and $\mathbf{R}_i$ have dimensions that depend on the number of fluid variables N_v considered.

Non-slip and adiabatic wall boundary conditions are imposed on the body surface as:

$$u = v = w = 0 \qquad \frac{\partial T}{\partial \mathbf{n}} = 0 \tag{3}$$

where $\mathbf{n}$ is the normal direction to the body surface and T stands for the temperature. At the external boundaries, a farfield boundary condition is used. The convective fluxes crossing the farfield boundary faces are calculated using the Advection Upstream Splitting Method (AUSM) Riemann solver and the flow conditions outside the boundary faces are determined employing Whitfield theory.

Additional information of DLR TAU-Code and details of the implementation can be found in Ref.[8].

2.2 Stability analysis

Stability analysis studies the growth or decay of perturbations superimposed onto a usually steady solution of the Navier-Stokes (NS) equations. The analysis can identify which particular features are prone to evolve under slight modifications of the flow conditions, either by introducing a perturbation or caused by a modification of some physical or geometrical parameters. The growth of these features would give rise to a completely

[1]Bold variables are used to refer vectors.

different flow configuration. Examples of the application of stability analysis to fluid dynamics problems can be found in the literature for a large variety of flow topologies [9, 10, 11].

Mathematically, the flow solution obtained through the RANS equations can be decomposed as:

$$\mathbf{q}(\mathbf{x},t) = \bar{\mathbf{q}}(\mathbf{x}) + \varepsilon\widetilde{\mathbf{q}}(\mathbf{x},t), \tag{4}$$

where $\varepsilon \ll 1$ and $\bar{\mathbf{q}}$ is the so called *base flow*, steady point of equilibrium of Eq. (2). Last term on the right hand side corresponds to small perturbations, prone to evolve and so time dependent.

This decomposition is introduced into the NS equations, Eq (2), and a Taylor series expansion is performed around the point of equilibrium $\bar{\mathbf{q}}$. Neglecting terms of order ε^2 and assembling all the unknowns in vector/matrix notation, it is obtained:

$$\varepsilon\mathbf{M}\frac{\partial\widetilde{\mathbf{q}}}{\partial t} = \mathbf{R}(\bar{\mathbf{q}}+\varepsilon\widetilde{\mathbf{q}}) \approx \mathbf{R}(\bar{\mathbf{q}}) + \varepsilon\left[\frac{\partial\mathbf{R}}{\partial\mathbf{q}}\right]_{\bar{\mathbf{q}}}\widetilde{\mathbf{q}}. \tag{5}$$

where the diagonal matrix $\mathbf{M}$, with leading dimension $N_v \times N$, contains the volumes associated to each cell and $\left[\frac{\partial\mathbf{R}}{\partial\mathbf{q}}\right]_{\bar{\mathbf{q}}}$ represents the jacobian matrix of the fluxes evaluated in the base flow.

The separability of temporal and spatial derivatives in (4) permits the introduction of an explicit harmonic temporal dependence of the disturbance quantities into these equations. In the Biglobal framework, considering pure two dimensional cases, the decomposition is accomplished according to the *ansatz*:

$$\widetilde{\mathbf{q}}(\mathbf{x},t) = \widehat{\mathbf{q}}(x,y)e^{\sigma t}, \tag{6}$$

where σ is a complex scalar and $\widehat{\mathbf{q}}$ describes the spatial complex disturbance. In pure two dimensional cases, the velocity component and all derivatives in the spanwise direction are neglected for both *base flow* and disturbances. Substitution of the *ansatz* given by equation (6) into the perturbed equation (5) and considering $\mathbf{R}(\bar{\mathbf{q}}) = 0$, equation (5) is transformed into the generalized eigenvalue problem:

$$\left[\frac{\partial\mathbf{R}}{\partial\mathbf{q}}\right]_{\bar{\mathbf{q}}}\widehat{\mathbf{q}} = \sigma\mathbf{M}\widehat{\mathbf{q}}, \tag{7}$$

which can also be expressed as:

$$\mathbf{A}\widehat{\mathbf{q}} = \sigma\mathbf{M}\widehat{\mathbf{q}}. \tag{8}$$

with $\mathbf{A} = \left[\frac{\partial\mathbf{R}}{\partial\mathbf{q}}\right]_{\mathbf{Q}}$ being the linearized jacobian matrix, and $\sigma = \sigma_r + i\sigma_i$ the complex eigenvalues of the generalized system. The real part of the eigenvalue, σ_r, refers to the amplification rate of the corresponding eigenmode, with the imaginary part σ_i being the pulsation, related to the associated frequency, f, as $\sigma_i = 2\pi f$.

2.3 Adjoint analysis

To obtain the adjoint operator, associated to the real non-symmetric operator $\mathbf{A}$, the following discrete inner product of a pair of continuous vectors, $\check{\mathbf{p}}$ and $\check{\mathbf{q}}$, is defined:

$$< \check{\mathbf{p}}, \check{\mathbf{q}} >= \int_{\Omega} \check{\mathbf{p}}^H \check{\mathbf{q}} d\Omega = \mathbf{p^H M q} \tag{9}$$

where H denotes the conjugate transpose, $\mathbf{p}$ and $\mathbf{q}$ are the discretized version of $\check{\mathbf{p}}$ and $\check{\mathbf{q}}$ in the computational domain Ω, and $\mathbf{M}$ is the volumes matrix previously defined.

Following this, the matrix $\mathbf{A}$ and its discrete adjoint $\mathbf{A}^+$ can be related as follows:

$$\begin{aligned} < \check{\mathbf{p}}, \mathbf{A}\check{\mathbf{q}} > &=< \mathbf{A}^+\check{\mathbf{p}}, \check{\mathbf{q}} >, \\ \mathbf{p}^H\mathbf{M}\mathbf{A}\mathbf{q} &= (\mathbf{A}^+\mathbf{p})^H\mathbf{M}\mathbf{q}, \\ \mathbf{p}^H\mathbf{M}\mathbf{A}\mathbf{q} &= \mathbf{p}^H(\mathbf{A}^+)^H\mathbf{M}\mathbf{q}, \\ \mathbf{M}\mathbf{A}\mathbf{M^{-1}} &= (\mathbf{A}^+)^H, \\ \mathbf{M^{-1}}\mathbf{A}^H\mathbf{M} &= \mathbf{A}^+, \end{aligned} \tag{10}$$

This expression relates the conjugate transpose of the jacobian matrix to its adjoint, allowing to obtain the associated adjoint eigenvalues, σ^+, and eigenmodes, $\mathbf{q}^+$:

$$\mathbf{A}^+\widehat{\mathbf{q}}^+ = \sigma^+\mathbf{M}\widehat{\mathbf{q}}^+ \tag{11}$$

2.4 Sensitivity analysis

The information contained in the adjoint modes can be used to evaluate the receptivity and sensitivity of the system. Giannetti and Luchini [12] introduced the concept of the 'wavemaker' for two-dimensional flows, showing that the areas of the flow more sensitive to structural changes, a localized force-velocity coupling, were localized on the overlapping regions of direct and adjoint modes. This defines the structural sensitivity as:

$$\mid \nabla\sigma \mid = \frac{\|\widehat{\mathbf{q}}^+\|\|\widehat{\mathbf{q}}\|}{< \widehat{\mathbf{q}}^+, \widehat{\mathbf{q}} >} \tag{12}$$

where $< \bullet, \bullet >$ denotes the discrete inner product, previously defined, and its associated norm $\| \bullet \| = < \bullet, \bullet >^{1/2}$. In this work, the adjoint modes have been normalized according to the condition $< \widehat{\mathbf{q}}^+, \widehat{\mathbf{q}} >= 1$.

Marquet et al. [13] studied the effects on the eigenvalue drift caused by a perturbation directly acting on the base flow equations. This context was developed afterwards in a discrete framework [14, 15], so is briefly described here. Following a Lagrangian approach [14], the sensitivity to base flow modifications can be calculated as:

$$\nabla_{\bar{\mathbf{q}}}\sigma = \mathbf{B}^+(\bar{\mathbf{q}}, \widehat{\mathbf{q}})\widehat{\mathbf{q}}^+ \tag{13}$$

where the matrix operator $\mathbf{B}$ is the sensitivity matrix, obtained through differentiating the jacobian matrix and the direct mode related to the eigenvalue of interest:

$$\mathbf{B}(\bar{\mathbf{q}}, \widehat{\mathbf{q}}) = \frac{\partial(\mathbf{A}(\bar{\mathbf{q}})\widehat{\mathbf{q}})}{\partial\bar{\mathbf{q}}} \tag{14}$$

This methodology can be extended to the application of a steady force, $\delta\mathbf{q_f}$, as an external perturbation, and the following sensitivity field is obtained:

$$\nabla_{\mathbf{q_f}}\sigma = \bar{\mathbf{q}}^{+} = (\mathbf{A}^{+}(\bar{\mathbf{q}}))^{-1}\nabla_{\bar{\mathbf{q}}}\sigma \tag{15}$$

being $\bar{\mathbf{q}}^{+}$ the adjoint of the base flow, obtained through the solving of the linear system.

3 NUMERICAL PROCEDURE

3.1 Base flow solver

The geometrical approximation is a simplification of the industrial problem, where only the details of the flow in the vicinity of the trailing edge of a turbine blade were studied. When the turbine passages and downstream stages are omitted, the blade trailing edge can be approximated by a simplified model as the supersonic flow over a flat plate blunt end. The geometry also includes the internal cooling passages, composed by a cavity plenum, where the purge flow was ejected, and the injector pipe, directly communicating the plenum with the base region.

The computational domain was limited by straight boundaries, with a length of $21.75\times d$ (with d as the trailing edge thickness) and a width of $20\times d$. The injector pipe had a length and width of $2.5\times d$ and $0.3\times d$, respectively. To keep subsonic conditions inside the cavity plenum, its width was kept three times larger than the injector pipe.

Boundary conditions of the control volume were defined as follows: supersonic inflow and output, Euler wall and symmetry plane were set at left, right, upper and lower limits respectively; non-slip wall was used for all internal surfaces and a reservoir-pressure inflow boundary condition was set to simulate the input of the cooling in the cavity plenum area.

The Mach number at the inflow boundary was set to 1.5, keeping a total temperature of 365 K and a Reynolds number of 9.4×10^6, based on the trailing edge length ($11.65\times d$). The flow rate at the cooling flow exit, from now on referred as the *blowing rate*, was defined by the cooling flow static temperature, kept to 300 K, and its total pressure, expressed as a percentage of the free stream flow total pressure.

Two types of simulations were performed on this work. When only half of the domain was simulated, a symmetry boundary condition was imposed on the axis of symmetry and then both mesh and solution were mirrored into the lower symmetry plane, to ensure a stability analysis over a symmetric *base flow* configuration. In order to understand the flow behaviour in non-symmetric configurations, simulations over the whole configuration were also completed. To clarify the exposition, when the term *half-domain* is used on this text, will refer to the mesh of Figure 2, with a symmetry plane on its lower boundary; on the contrary, when *full-domain* is called, it will refer to simulations done on a mirrored mesh, considering upper and lower surfaces of the trailing edge.

The domain was discretized using a quad-structured mesh, generated using an O-Grid topology and dividing the geometry into regions of interest. Wall normal grid distances were set small enough so values of y^+ lower than 1 were kept on the body surfaces. Mesh details are depicted on Figure 2. The mesh spatial resolution was concentrated at the contraction-expansion and around the shock wave areas.

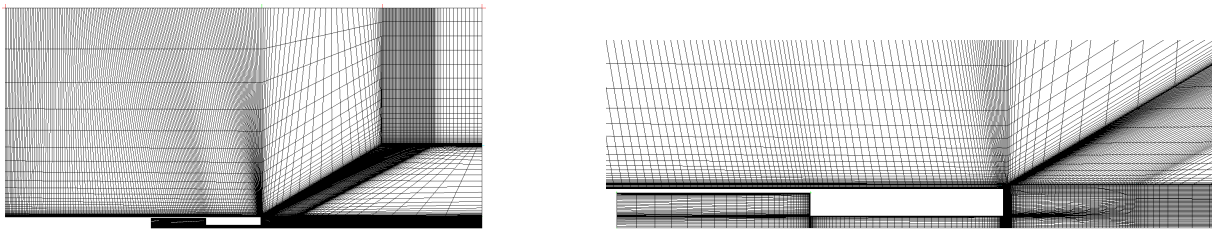

(a) Computational mesh

(b) Cavity and channel area mesh detail

Figure 2: Computational mesh. Only a quarter of total nodes are shown for clarity.

Table 1: Mesh convergence analysis for a blowing rate of 18%. P_b/P_b^* represents the relation between the pressure measured at the base region with and without purge flow applied, and ρ_{purge}/ρ_f the relation between the density values at the cavity plenum and at the base region.

Mesh	Number of nodes	P_b/P_b^*	ρ_{purge}/ρ_f
M1	12010	1.26932202	1.03157676
M2	48260	1.29883128	1.03038449
M3	104630	1.30545566	1.02675552
M4	207106	1.31826117	1.01727924
M5	321090	1.31929642	1.01407829
M6	424640	1.31858961	1.01426252

A mesh convergence study was performed for a blowing rate of 18% for a half-domain configuration using six different meshes of increasing number of elements, named from M1 to M6. A systematic refinement was performed to evaluate the flow sensitivity to the mesh density. At each step the mesh was refined increasing n times the number of nodes, taking the mesh M1 as the reference. This refinement law preserved the topology of the mesh and guaranteed that Richardson extrapolation formulas were applicable to obtain an accurate rate of convergence. The convergence criteria of the RANS simulations, evaluated through the global density residual, was set up to values lower than 10^{-6}.

Detailed results from the mesh convergence study are shown in Table 1. For each mesh the pressure and density values at the trailing edge were monitored. According to these results, mesh M4 was selected as a good compromise between accuracy and computational efficiency.

3.2 Eigenvalue problem solving

The real non-symmetric operator $\mathbf{A}$ (Eq. 7) and the real diagonal operator $\mathbf{M}$ were directly extracted from the solver, using the first-discretize-then-linearize technique implemented in the DLR-TAU solver. For the particular case of mesh M4, the leading dimension of the matrix $\mathbf{A}$ was approximately 1.2×10^6, and the number of non-zero elements was 9.6×10^7.

For each eigenvalue the associated eigenvector that represents the underlying physical feature (density, momentum in the spatial directions (x, y, z), energy and turbulent components), will decay or eventually grow in time depending on the sign of the real

part of the eigenvalue. To calculate the eigenvalues and eigenvectors of system 8, the Implicitly Restarted Arnoldi Method (IRAM) algorithm implemented in the ARPACK library [16] combined with a shift-and-invert preconditioning technique was used. Not all the eigenvalues were computed, but only a finite number close to the area of interest of the eigenspectra. At each iteration of the IRAM algorithm, the shift-and-invert method requires the inversion of a linear system, which makes this procedure computationally expensive. Moreover, due to the stiffness associated to the underlying compressible and turbulent equation system, the jacobian matrix $\mathbf{A}$ is bad conditioned, so iterative methods to solve the linear system fail to reach a proper convergence. In this work, a full LU factorization was performed for the Jacobian matrix $\mathbf{A}$ using the MUMPS library [17]. This strategy, used here in a compressible finite volume context, has also been followed in stability analysis of incompressible flows in finite elements discretizations and in the context of spectral methods [18, 19, 14] and highly compressible flows with turbulence modelling [6]. Unfortunately, the full LU decomposition scales as the cube of the number of unknowns ($(N_v \times N)^3$), becoming the bottleneck of the overall process and consuming a large amount of computational resources [6]. To partially redice this requirement, the sparsity of the jacobian matrix was exploited on the parallelization of the algorithms and domain reduction techniques [20] were implemented to alleviate the computational resources required for the stability analysis.

4 RESULTS

4.1 Flow topology analysis

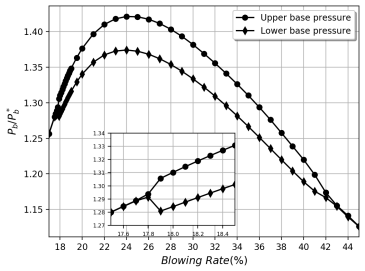

Figure 3: Base pressure as a function of the blowing rate.

The ratio between the computed base pressure at both sides of the trailing edge (P_b) and the base pressure for a non-blowing configuration (P_b^*) is shown as a function of the blowing rate (Figure 3). Pressure values bifurcate for a blowing rate of 17.8%, going back to the symmetric flow state for a blowing rate of 42% and reaching a maximum value of a 3.6% of pressure difference at 28% of blowing intensity. The value of the blowing rate for the maximum pressure difference does not match the maximum value for the base pressure, which takes place at a blowing rate of 24%. As it will be shown, the reason of this behavior is the appearance of a non-symmetric global mode that eventually becomes unstable and dominates the flow configuration. With the aim of capturing the instability related with the onset of this bifurcation and identifying the sources of the non-symmetry, blowing rate values from 10% to 45% were investigated.

Base flow pressure and velocity fields for a half-domain configuration, including the solution for a non-blowing configuration, are displayed in figures 4 and 5. These figures reveal how the shock waves decrease their intensity for low purge intensities, which combined with the filling effect of the purge jet increase the pressure of the base region. For

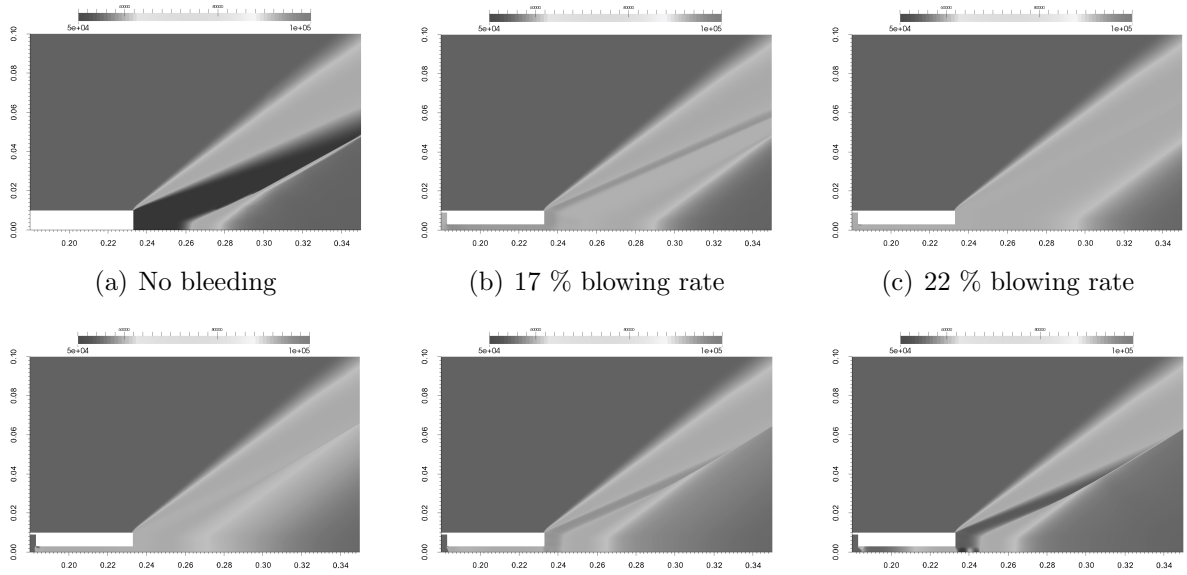

(a) No bleeding (b) 17 % blowing rate (c) 22 % blowing rate

(d) 31 % blowing rate (e) 37 % blowing rate (f) 43 % blowing rate

Figure 4: Pressure contours of RANS solutions for a set of blowing rate intensities.

blowing rates values higher than 24%, the flow on the dead area starts to evacuate and the pressure at the base region decays, recovering the shock part of its original strength.

A detailed evolution of the re-circulation areas is shown on Figure 6, where only negatives velocities from full-domain RANS solutions are plotted. As the jet is applied at the base region, the main recirculation area is pushed downstream and split in three regions, two at the trailing edge tips and a third one downstream. However, for blowing ratios above the bifurcation point, one of the trailing edge recirculation areas joins the downstream one, increasing the pressure on that side and forcing the flow to change its direction in a *Coanda effect* style and hit the shear layer. This change alters the wake structure, affecting the shocks angles and intensities. Larger blowing rates, however, stabilize the flow pushing the dead air zones towards the symmetry plane as more flow is entrained into the main jet until the symmetric state is achieved again. The non-symmetric effect can also be appreciated from shadow-graph contour fields shown in Figure 7, where it is easier to identify the weakening of the trailing edge shock wave and the appearance of a secondary upstream shock only in one side of the domain. The secondary upstream shock has its foot near the region where the purging flow contacts the trailing edge shear layers. If the flow changes its direction and deflects to the contrary side, the secondary shock will swap side as well.

4.2 Stability analysis

On Saracoglu et al.[5], the pressure measurements were done over URANS solutions, showing an asymmetrical state that was constant in time. This could suggest that the difference on pressure had not a periodic oscillation behavior but a steady one. As shown on the flow topology analysis (Sec 4.1), the cooling flow experiments a contraction at the

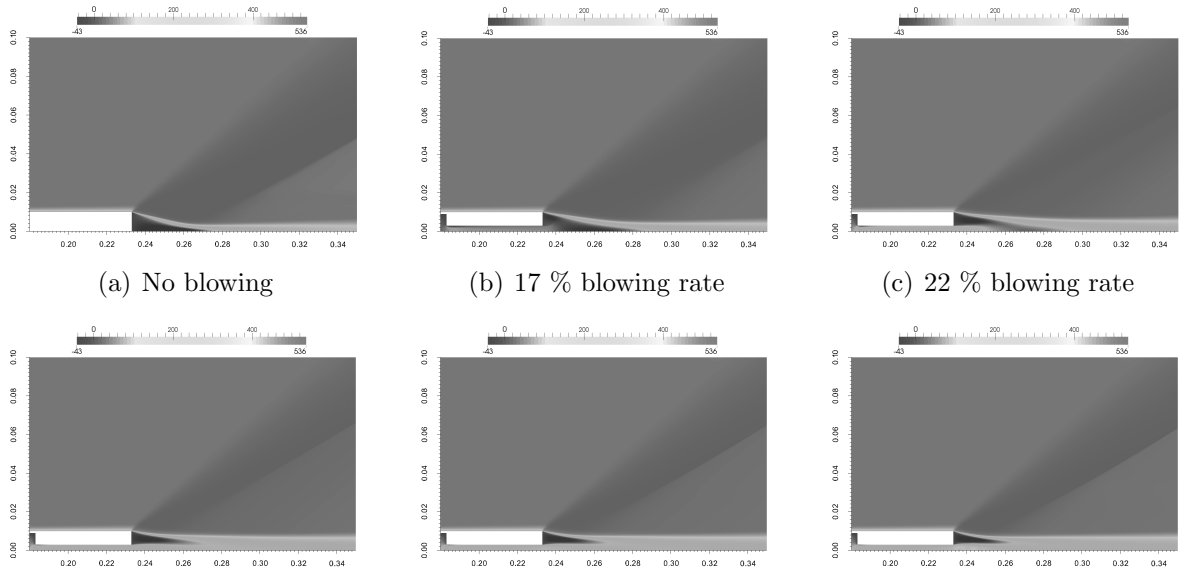

(a) No blowing (b) 17 % blowing rate (c) 22 % blowing rate

(d) 31 % blowing rate (e) 37 % blowing rate (f) 43 % blowing rate

Figure 5: Streamwise velocity contours of RANS solutions for a set of blowing rate intensities.

plenum area, followed by a sudden expansion at the base region, limited on the upper and lower sides by the shear layers. According to the type of perturbation observed on the base flow (Fig. 3-(a)), the geometry configuration and the results of Saracoglu [5], it would be expected to find the physical eigenvalues on the imaginary axis, having a null pulsation. This kind of instability, known as a pitchfork bifurcation, would led to a steady asymmetric behavior of the recirculation regions at the trailing edge. Therefore, the focus was set on the region of the spectrum close to the origin and a zero value for the shift parameter was used on the preconditioning of the jacobian matrix.

As previously explained, the base flow was computed using the half-domain mesh whereas for the stability analysis the full-domain mesh was used. Density, momentum, energy and turbulent components of the perturbation fields were obtained from the anal-

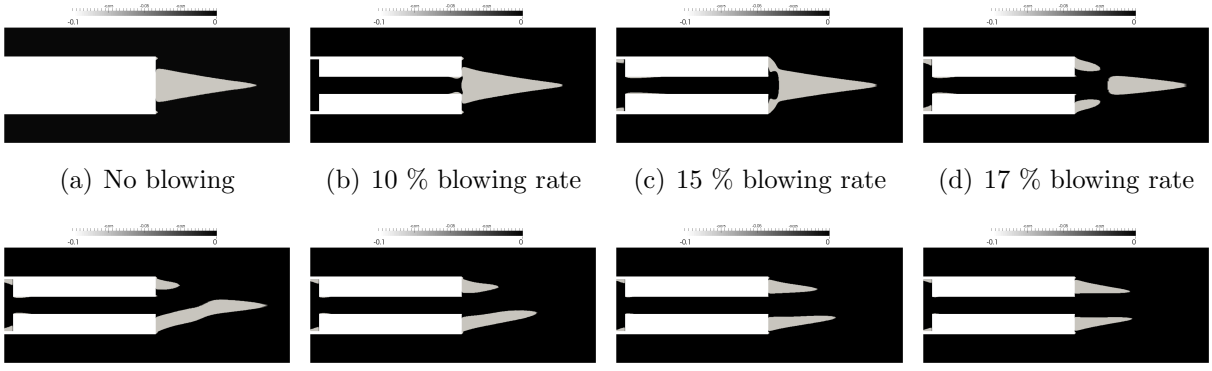

(a) No blowing (b) 10 % blowing rate (c) 15 % blowing rate (d) 17 % blowing rate

(e) 18 % blowing rate (f) 22 % blowing rate (g) 33 % blowing rate (h) 42 % blowing rate

Figure 6: Dead air regions for a set of blowing rate intensities. Only negative velocities are plotted.

ysis.

For blowing rates below 18%, all the eigenvalues of the spectrum remain on the stable region. When the blowing rate is increased, a single anti-symmetrical mode becomes unstable and its growth rate evolves as a function of this parameter. This mode is directly related to the pressure bifurcation, its associate eigenvalue crossing the imaginary axis when the purge intensity is above 18.1%, and becoming stable again for a blowing rate of 38% (Fig. 8). When the eigenvalue evolution is related to the base flow results, it can be observed that as the base region experiments changes on its flow topology, the real part of the unstable eigenvalue reaches its maximum value. This coincides with an enlargement of the recirculation bubbles of the trailing edge and an increment of the pressure drop at the wake (as shown in Figures 4 and 6). After this point, the eigenvalue starts its damping until a blowing rate value of 38%, where it becomes stable again at the same time the base flow recovers its symmetric state.

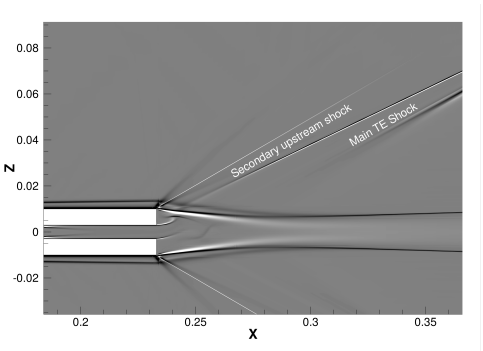

(a) 18 % blowing rate

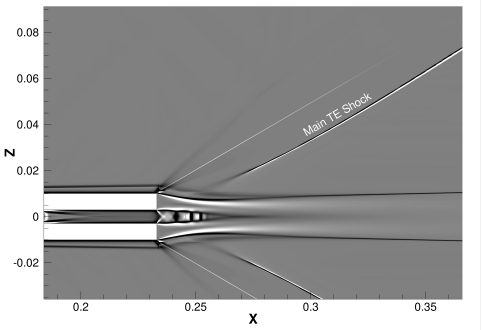

(b) 45 % blowing rate

Figure 7: Shadowgraph contours for non-symmetric (a) and symmetric (b) flow configurations.

The eigenmode structure consists in two symmetrical lobe-shaped regions with anti-symmetrical streamwise perturbation components, and it changes its structure as the blowing rate increases, in consonance with the flow topology of the base flow (Fig. 9). For lower purge intensity cases, the mode appears concentrated at the exit of the purge channel and associated to the weak shear layers that occur on the mixing of the base region and the purge flow. Subsequently, for larger blowing rates the mode changes its shape becoming more similar to the structures observed in common channel expansions [21], where it adopts the shape of two enlarged lobes bounded by the strong shear layers of the upper and lower tips of the trailing edge.

The behavior of the amplification rate is different for low and high blowing intensities. For a weak trailing edge blowing, the rate of change of the amplification of the mode is high, and small variations of blowing rates would produce a rapid change of the global mode behavior from stable to unstable. At higher blowing rates the tendency is smoother and the changes in stability become less abrupt. This fact can also explain the small differences between the RANS results and the stability analysis. Namely, according to RANS computations, the flow remains non-symmetric until a blowing rate of around 42%, compared to a value of 38% for the stability analysis. However, it is normally observed that, when the growth rate of the instability is not large enough, the flow can remain

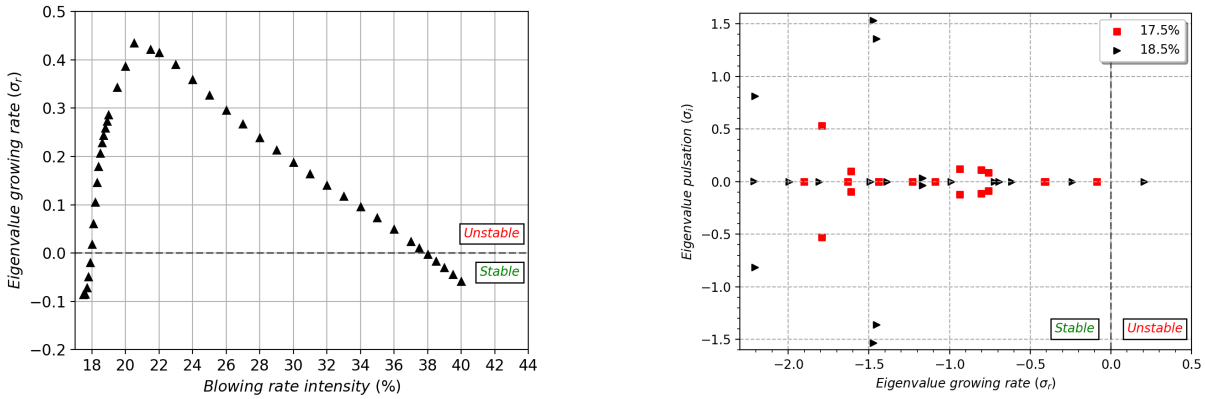

(a) Evolution of the leading eigenvalue with the blowing rate

(b) Comparison of the spectra for stable (17.5%) and unstable (18.5%) configurations.

Figure 8: Eigenvalue analysis.

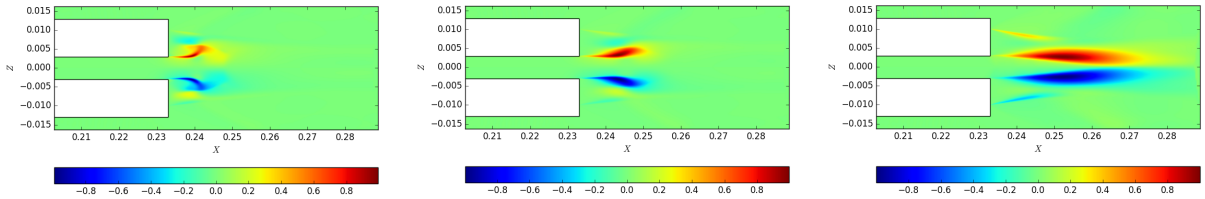

(a) 18 % blowing rate

(b) 20 % blowing rate

(c) 40 % blowing rate

Figure 9: Eigenmode evolution with the blowing rate.

in a "unstable" situation for a long time, unless a perturbation is introduced in the flow triggering the new flow configuration [22].

4.3 Sensitivity to structural and steady forcing modifications

The overlapping of direct and adjoint modes permits the calculation of the so called 'structural sensitivity', associated to the regions where structural modifications of the flow would have a major effect on the instability of the global mode. These regions represent the instability core, and they appear symmetric respect to the mid plane and close to the end of the purge channel, coincident with the weak shear layers formed from the mixing of the cooling jet and the trailing edge recirculation areas. Results of the sensitivity analysis for a blowing rate of 30% are shown in Figure 4.3. Small differences were found for changes in the blowing rate intensity.

The sensitivity to a steady force, normally represented by a complex vector field, is here constructed only by its real part due to the stationary nature of the unstable global mode. The information provided by the vector field indicates where an arbitrary modification $\delta\mathbf{q_f}$ applied in the direction of the growth rate sensitivity will have a greater destabilization impact on the behavior of the eigenmode. The global mode related with the pressure bifurcation seems to be more sensitive in the mixing region, and downstream from the

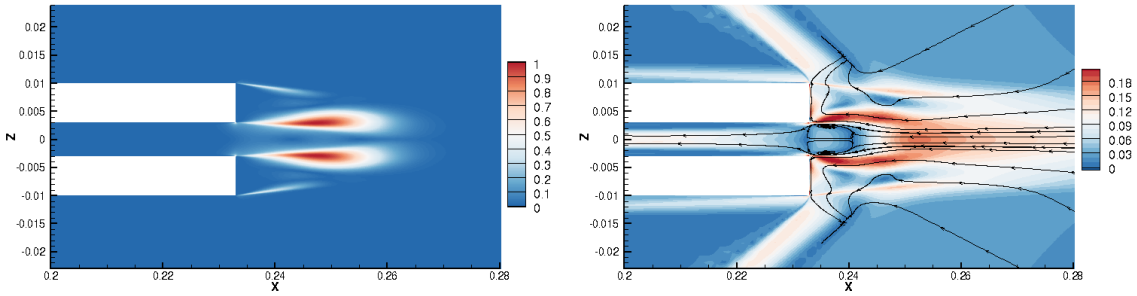

Figure 10: Structural sensitivity of the unstable global mode (left), and sensitivity to a steady force (right). Data corresponds to a blowing rate of 30%.

end of the channel (Figure 4.3-right). Except on the small area limited by the shear layers, the presence of a steady force applied with a reverse direction to the discharging flow will have a destabilinzing effect on the eigenvalue. Perturbations with a vertical component applied close to the trailing edge surface could have a stabilizing effect if they are directed from the trailing edge tip towards the discharging channel.

5 CONCLUSIONS

A simple model of the flow configuration in the vicinity of a cooled engine turbine blade trailing edge has been analyzed with a combination of RANS and stability analysis. The presence of a bifurcation changing from a symmetric to non-symmetric pressure distribution on the base region as a function of the jet blowing rate had been observed but not explained before. Previous analysis suggested that the observed bifurcation could be generated by a sudden expansion mechanism [5]. This fact has been confirmed on this work with the use of Global Stability Theory.

The results link the non-symmetrical configuration with an anti-symmetric eigenmode for a range of blowing rates, matching the start and end points of the pressure bifurcation with the stability behavior of the associated eigenvalue, with small error when compared with RANS results. An error value of 0.5% was found for low blowing rates, with an error of about 5% for higher blowing rates. The eigenmode flow structures appeared to extend downstream in space as the purge intensity increased, revealing itself as a clear sudden expansion mode [21] for higher blowing rates, but more concentrated at the end of the cooling channel for lower blowing rates. It is on this range of blowing rates where the mode takes an structure more opened to the lower and upper sides, in a shear layer shape, and where it is more sensitive to changes in the blowing rate.

Base pressure magnitude inversely correlated with trailing edge shock intensity. Due to the destabilizing effect of the pressure bifurcation, the range of blowing intensities related to maximum base pressure values was affected by a variation on the pressure values of upper and lower sides at the trailing edge. The pressure bifurcation could had a strong effect on the surrounding flow topology and adjacent blades of the turbine, due to the pressence of a secondary shock wave upstream the main trailing edge shock wave, that appears for blowing rates comprised between 18 and 38% (Fig. 7). This additional

shock system, placed in only one side of the blade, would change to the opposite side when the deflected purge flow changed its direction due to a bifurcation branch change, generating additional non-symmetrical loads on the turbine cascade. If this intermittent shock system is replicated all over the turbine blades, considering independent changes and interactions with upstream and downstream stages of the turbine, the consequences in the aerodynamic loads can be very important. The non time dependent nature of the instability would made it difficult to be controlled by frequency modulated systems [3], but may be suitable for passive control or upstream flow modulation. To exploit these capabilities, a sensitivity analysis was performed over the unstable global mode. The instability core appeared to be located in the mixing region area, as two symmetric lobes. The information extracted from the sensitivity to steady forcing showed that, generally, a perturbation in the mixing regions of the cooling flow and the low-momentum base region in the direction of the cooling flow flow would have a stabilizing effect on the eigenvalue. However, despite the area of the base region located at the end of the cooling channel is less sensitive to modifications, perturbations in this area in the direction of the flow will have a destabilizing effect.

ACKNOWLEDGMENTS

This research was carried out under the project SSeMID, which has received funding from the European Union Horizon2020 research and innovation programme under the Marie Skodowska-Curie grant agreement No 675008.

REFERENCES

[1] Paniagua, G., Yasa, T., La Loma, A. D., Castillon, L., and Coton, T., "Unsteady Strong Shock Interactions in a Transonic Turbine: Experimental and Numerical Analysis," *Journal of Propulsion and Power*, Vol. 24, No. 4, jul 2008, pp. 722–731.

[2] Denton, J. D. and Xu, L., "The Trailing Edge Loss of Transonic Turbine Blades," *Journal of Turbomachinery*, Vol. 112, No. 2, 1990, pp. 277–285.

[3] Saracoglu, B. H., Paniagua, G., Salvadori, S., Tomasoni, F., Duni, S., Yasa, T., and Miranda, A., "Trailing edge shock modulation by pulsating coolant ejection," *Applied Thermal Engineering*, Vol. 48, 2012, pp. 1–10.

[4] Raffel, M. and Kost, F., "Investigation of aerodynamic effects of coolant ejection at the trailing edge of a turbine blade model by PIV and pressure measurements," *Experiments in Fluids*, Vol. 24, No. 5-6, 1998, pp. 447–461.

[5] Saracoglu, B. H., Paniagua, G., Sanchez, J., and Rambaud, P., "Effects of blunt trailing edge flow discharge in supersonic regime," *Computers and Fluids*, Vol. 88, 2013, pp. 200–209.

[6] Iorio, M. C., González, L. M., and Ferrer, E., "Direct and adjoint global stability analysis of turbulent transonic flows over a NACA0012 profile," *International Journal for Numerical Methods in Fluids*, Vol. 76, No. 3, 2014, pp. 147–168.

[7] Grilli, M., Schmid, P. J., Hickel, S., and Adams, N. A., "Analysis of unsteady behaviour in shockwave turbulent boundary layer interaction," *Journal of Fluid Mechanics J. Fluid Mech*, Vol. 700, No. 700, 2012, pp. 16–28.

[8] Institute of Aerodynamics and Flow Technology (DLR), "Technical Documentation of the DLR TAU-Code Release 2016.2.0." 2016.

[9] Meseguer-Garrido, F., de Vicente, J., Valero, E., and Theofilis, V., "On linear instability mechanisms in incompressible open cavity flow," *Journal of Fluid Mechanics*, Vol. 752, No. 2014, 2014, pp. 219–236.

[10] González, L. M., Ahmed, M., Kühnen, J., Kuhlmann, H., and Theofilis, V., "Three-dimensional flow instability in a lid-driven isosceles triangular cavity," *J. Fluid Mech*, Vol. 675, 2011, pp. 369–396.

[11] Iorio, M. C., González, L. M., and Martinez-Cava, A., "Global Stability Analysis of a Compressible Turbulent Flow around a High-Lift Configuration," *AIAA Journal*, Vol. 54, No. 2, 2015, pp. 373–385.

[12] Giannetti, F. and Luchini, P., "Structural sensitivity of the first instability of the cylinder wake," *Journal of Fluid Mechanics*, Vol. 581, 2007, pp. 167.

[13] Marquet, O., Sipp, D., and Jacquin, L., "Sensitivity analysis and passive control of cylinder flow," *Journal of Fluid Mechanics*, Vol. 615, No. 2008, 2008, pp. 221–252.

[14] Browne, O. M. F., Rubio, G., Ferrer, E., and Valero, E., "Sensitivity analysis to unsteady perturbations of complex flows: a discrete approach," *International Journal for Numerical Methods in Fluids*, Vol. 76, No. 12, dec 2014, pp. 1088–1110.

[15] Mettot, C., Renac, F., and Sipp, D., "Computation of eigenvalue sensitivity to base flow modifications in a discrete framework: Application to open-loop control," *Journal of Computational Physics*, Vol. 269, 2014, pp. 234–258.

[16] Lehoucq, R. B., Sorensen, D. C., and Yang, C., "ARPACK Users Guide: Solution of Large Scale Eigenvalue Problems by Implicitly Restarted Arnoldi Methods." 1997.

[17] Amestoy, P. R., Duff, I. S., L'Excellent, J.-Y., and Koster, J., "A Fully Asynchronous Multifrontal Solver Using Distributed Dynamic Scheduling," *SIAM Journal on Matrix Analysis and Applications*, Vol. 23, No. 1, jan 2001, pp. 15–41.

[18] De Vicente, J., Rodríguez, D., Theofilis, V., and Valero, E., "Stability analysis in spanwise-periodic double-sided lid-driven cavity flows with complex cross-sectional profiles," *Computers and Fluids*, Vol. 43, No. 1, 2011, pp. 143–153.

[19] Ferrer, E., de Vicente, J., and Valero, E., "Low cost 3D global instability analysis and flow sensitivity based on dynamic mode decomposition and high-order numerical tools," *International Journal for Numerical Methods in Fluids*, Vol. 76, No. 3, sep 2014, pp. 169–184.

[20] Sanvido, S., Garicano-Mena, J., de Vicente, J., and Valero, E., "Critical Assessment of Domain Reduction Strategies for Global Stability Analisis," *AIAA*, 2017.

[21] Fani, A., Camarri, S., and Salvetti, M. V., "Stability analysis and control of the flow in a symmetric channel with a sudden expansion," *Physics of Fluids*, Vol. 24, No. 8, aug 2012, pp. 084102.

[22] Valero, E., Ferrer, E., and de Vicente, J., "Numerical Methods for Direct Numerical Simulation and Stability Analysis," *VKI Lecture Series 2014*, 2014.